Effect of O-spacer layer in the interaction between graphene and graphone with a ferromagnetic metal substrate

IISER PUNE

A thesis submitted towards partial fulfilment of

BS-MS Dual Degree Programme

by

C GAURAV

under the guidance of

DR. PRASENJIT GHOSH

INDIAN INSTITUTE OF SCIENCE EDUCATION AND RESEARCH PUNE

Certificate

This is to certify that this thesis entitled "**Effect of O-spacer layer in the interaction between graphene and graphone with a ferromagnetic metal substrate**" submitted towards the partial fulfilment of the BS-MS dual degree programme at the Indian Institute of Science Education and Research Pune represents original research carried out by C Gaurav at Indian Institute of Science Education and Research -Pune, under the supervision of Dr. Prasenjit Ghosh during the academic year 2013-2014.

Student

C GAURAV

Supervisor

PRASENJIT

GHOSH

Acknowledgements

I would like to thank my guide Dr. Prasenjit Ghosh. He encouraged me throughout and gave me all possible freedom. He was patient with me at difficult times.

Also I would like to thank my lab mates. I enjoyed my stay in the lab and was happy having different kind of discussions with them. In particular, I would like to thank Niharika Joshi for always being there for me and helping me throughout my project.

Abstract

Using ab initio density functional theory, we have studied the electronic and magnetic properties of graphene and semi-hydrogenated graphene supported on oxygen adsorbed Ni(111) surface. For the mono-layer coverage of oxygen atoms it is observed that the oxygen intercalation decouples graphene from Ni(111)-O substrate and the Dirac cone at K point shifted above the Fermi energy. Interaction of semi-hydrogenated graphene is stronger with Ni(111)-O as compared to clean Ni(111)-O surface. A five-fold increase in magnetic moment of surface Ni atoms is observed. For the half mono-layer coverage of oxygen it is seen that that induced magnetic moment on graphene increases significantly.

Contents

Chapter 1

Introduction

Magnetism is usually associated with systems having unpaired localized d or f electrons. However, recent studies have shown that certain modified forms of graphene (s and p electrons) also possess magnetic properties. Graphene is a 2-dimensional sheet of sp^2 hybridized carbon atoms forming a honeycomb lattice. Even though the theoretical studies of graphene has been going on for quite long, it was only in 2004 that Geim and Novoselov could isolate the 2-d sheets of graphene with an adhesive tape.[1].

Graphene has two carbon-carbon bonds, namely σ and π. The valance shell configuration for carbon atom is $2s^2$,$2p_x^1$,$2p_y^1$. In the sp^2 hybridization, the s, p_x and p_y form three σ bonds in the plane of the sheet and p_z orbitals forms a π bond in the direction perpendicular to the sheet, as shown in Fig.1(a). The σ bond is responsible for the large binding energy and elastic properties while the π bond gives rise to interesting electronic properties of graphene.The bonding and anti-bonding orbitals of σ bond has a very large energy gap of $\sim$ 12 eV. On the contrary, the bonding and anti-bonding states of π bond have energy levels near Fermi level(E_F).

Graphene is a semi-metal. The lattice of graphene can be seen as two interpenetrating triangular lattices with two atoms per unit cell (fig 1(a)). Within the assumption of nearest neighbor coupling in the tight binding model [2], the dispersion relation for graphene is shown in fig 1(b). At the K point of the Brillouin zone (BZ) graphene shows a linear dispersion.[3].
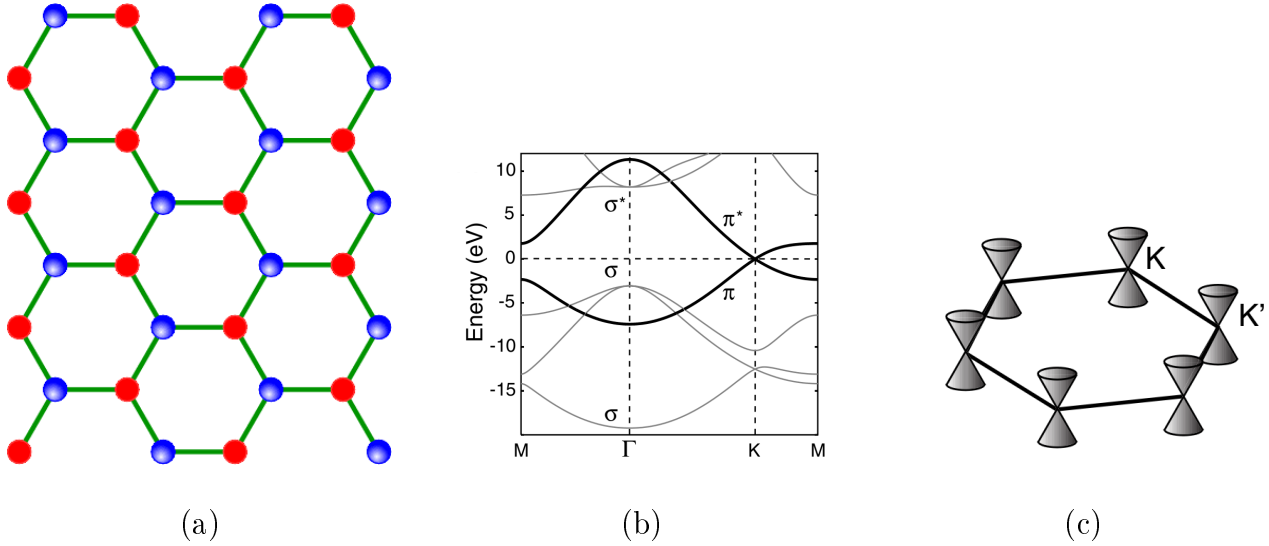
Figure 1.1: (a) Two-dimensional crystalline lattice of graphene. (b) Band structure of graphene obtained by means of first-principles calculations. The bands are labeled according to their symmetry. The zero energy corresponds to the Fermi level. (c) Dirac cones of graphene in the hexagonal Brillouin zone. [G M Sipahi *et al J. Phys.: Condens. Matter* 26 104204 (2014)]

The charge carriers in graphene can travel ballistically over great distances without scattering. Moreover, its unique electronic structure gives rise to exceptional transport and spin-filtering properties,[4]. These unusual electronic properties make graphene a promising candidate for future nano-electronics. However, graphene is a semi-metal with the conduction and valence band forming the Dirac cone at the K-point of the Brillouin zone (BZ). To use graphene as a material for semiconductor spintronics, it is desirable not only to make graphene magnetic but also to open up the band gap.

Chemical functionalization of graphene is an effective way in which the electronic and magnetic properties of graphene can be modified. For instance, hydrogenating the free-standing graphene makes it an insulator [5] while semi-hydrogenation of the graphene sheet turns it into a ferromagnetic semiconductor [6]. Moreover, for any device application of graphene, making contacts with metals is necessary. In this perspective, growth of graphene on Ni(111) and Co(0001) surfaces is of particular interest since there is almost perfect lattice matching between the substrate and the graphene sheet. This minimizes the effect of strain on the supported graphene sheet.

Studies have been done to understand the electronic and magnetic properties of graphene supported on Ni(111) surface [7] which show that there is a small induced magnetic moment

on graphene and the band gap at the K point opens up. The graphene becomes ferrimagnetic with the average magnetic moment of the clean graphene sheet aligned parallel to that of the surface Ni atoms. Upon hydrogenation of the graphene sheet the magnetic moment of graphene increases and the band gap at the K point increases further.

The interaction between the graphene sheet and the substrate can be modified by introducing atoms like Fe, O etc between the graphene sheet and the substrate. Using ab initio density functional theory calculations we study how intercalation of oxygen effects the electronic properties of the supported graphene and semi-hydrogenated graphene (Graphone).

Chapter 2

Theoretical Methods

2.1 Introduction

Calculations of the electronic structure of a material give us microscopic insight into its structural, mechanical and microscopic properties. The structure and properties of a system can be calculated once we solve the Schrödinger equation which is given as :

$$H\Psi = E\Psi \tag{2.1}$$

where Ψ is the many body wave function and is a function of the positions of the electrons and nuclei which constitute the system, E is the eigenvalue and H is the Hamiltonian of the system. Let us denote the position and momentum of the ith nucleus by $\mathbf{R}_i$ and $\mathbf{P}_i$, respectively, and of j th electron by $\mathbf{r}_j$ and $\mathbf{p}_j$. The mass of each nucleus be M and nuclear charge be Z_e. The total Hamiltonian is as follows:

$$H = -\sum_{i=1}^{N} \frac{\hbar^2}{2M_i}\nabla_i^2 + \frac{-\hbar^2}{2m}\sum_{j=1}^{n}\nabla_j^2 + \frac{(Ze)^2}{2}\sum_{i,i'}\frac{1}{|\mathbf{R}_i-\mathbf{R}_{i'}|} + \sum_{j,j'}(\frac{e^2}{2})\frac{1}{|\mathbf{r}_j-\mathbf{r}_{j'}|} - Ze^2\sum_{i,j}\frac{1}{|\mathbf{r}_j-\mathbf{R}_i|} \tag{2.2}$$

The first two terms correspond to the kinetic energy of the nuclei and the electrons (T_N and T_e) respectively. The third and fourth terms are the nuclei- nuclei (V_{NN}) and electron-electron (V_{ee}) repulsion energy and the last term is the electron-nuclei attractive potential energy (V_{eN}).

$$(T_N + T_e + V_{NN} + V_{ee} + V_{eN})\Psi(\mathbf{R}, \mathbf{r}) = E\Psi(\mathbf{R}, \mathbf{r}) \tag{2.3}$$

where $\Psi(\mathbf{R}, \mathbf{r})$ is the many-body wave function.

2.2   The Born-Oppenheimer Approximation

In the Hamiltonian though the KE terms are one-body terms, the potential energy terms being two-body interactions makes it impossible to solve it exactly. However, the equation can be simplified by taking advantage of difference in masses of electron and nuclei. Since the nuclei are much more heavy than electrons they move much slower than the electrons(typical ratio M/m is $\sim$ 2000 or more). As a result, the nucleus can be approximated to be static related to electrons and we can consider the electrons as moving in the background field of fixed nuclei. This is called as **Born** − **Oppenheimer** or *adiabatic* approximation.[8]. This allows the decoupling of nucleus and electron degrees of freedom.The wave function can be written as product of wave functions of electronic and nuclear components.

$$\Psi = \psi_{nuclear} * \psi_{elec} \tag{2.4}$$

Assuming first that the nuclei are fixed we can solve for electron motion. Under this framework, nuclear kinetic energy can be assumed to be zero and their potential energy (V_{NN}) is basically a constant for a given configuration. Hence the electrons move in a static potential background provided by the static ions.

The Schrödinger equation (electronic part) becomes:

$$\left(\frac{-\hbar^2}{2m} \sum_{j=1}^{n} \nabla_j^2 + \sum_{j,j'} (\frac{e^2}{2}) \frac{1}{|\mathbf{r}_j - \mathbf{r}_{j'}|} - Ze^2 \sum_{i,j} \frac{1}{|\mathbf{r}_j - \mathbf{R}_i|} \right) \psi_{elec}(r_k) = E_{elec}(R_i)\psi_{elec}(r_k)$$

(2.5)

Once the electronic part is solved for a fixed position of ions, the ionic part may now be obtained from:

$$\left(-\sum_{i=1}^{N} \frac{\hbar^2}{2M_i} \nabla_i^2 + \frac{(Ze)^2}{2} \sum_{i,i'} \frac{1}{|\mathbf{R}_i - \mathbf{R}_{i'}|} + E_{elec}(R_i) \right) \psi_{ionic}(R_i) = E_{tot}\psi_{ionic}(R_i) \qquad (2.6)$$

Here,

$$E_{tot} = E_{elec} + E_{nuc} \qquad (2.7)$$

The electronic contribution gives rise to an effective attractive potential between ions which leads to bonding.

2.3   The Hohenberg-Kohn Theorem

The Born-Oppenheimer approximation helps in successfully separating the electronic and nuclei degrees of freedom. However, the electron-electron repulsion term is still almost impossible to solve in the many-body Hamiltonian. This is where Density functional theory comes into play. In 1964 Hohenberg and Kohn stated the famous **Hohenberg − Kohntheorem** which states that:

"For any system of interacting particle in external potential V(r), the potential V(r) is determined uniquely, except for a constant, by the ground state particle density $n_0(r)$."[9].

Let there be a many body Hamiltonian H;

$$H = T + U + V \qquad (2.8)$$

Here T is the kinetic energy, U is the electron-electron interaction and V, the external

8

potential. Let the ground state wave function be ψ. The charge density is defined as

$$n(r) = N|\psi(r, r_2, r_3, ... r_N)|^2 dr_2 ... r_N \qquad (2.9)$$

Now,let us consider a different Hamiltonian H' as given below and let corresponding ground state wave function be ψ'.

$$H' = T + U + V' \qquad (2.10)$$

V and V' do not just differ by a constant. Another assumption we take is that both the cases have same ground state density i.e. n(V) = n(V'). As a consequence we get the following inequality.

$$E' = \langle \psi'|H'|\psi' \rangle$$

$$< \langle \psi|H'|\psi \rangle$$
$$= \langle \psi|H|\psi \rangle + \langle \psi|H' - H|\psi \rangle$$
$$= \text{E} + \int dr n(r)[V(r) - V'(r)] (2.11)$$

Similarly we can show that,

$$E < E' + \int dr n(r)[V(r) - V'(r)]$$

(2.12)

Summation of the above two inequalities leads to the contradiction

$$E + E' < E + E' \qquad (2.13)$$

Hence the assumption of identical density arising from the two different external potentials

is wrong. Thus a given n(r) can only correspond to only one V(r) and, the Hamiltonian and the wave functions are also fixed by density n(r). Since the wave function is a functional of density, the energy functional $E_v[n]$ for a given external potential V(r) is a unique functional of density.

2.4 The Hohenberg-Kohn variational theorem

The kinetic and potential energies can be written as a functional of n(r). Now an universal functional can be defined,

$$F[n] = \langle \Psi | T + U | \Psi \rangle \tag{2.14}$$

which is valid for any number of any number of particles and any external potential. Now, for a given external potential $v(r)$ the energy functional is,

$$E_v[n] = \int v(r)n(r)d(r) + F[n] \tag{2.15}$$

The Hohenberg-Kohn variational theorem states that for every trial density function n_{tr} (r) that satisfies the conditions, $\int n_{tr}$ (r)dr = N and $n_{tr}(r) \geq 0$ for all r, the following inequality holds: $E_0 \leq E_v [n_{tr}]$ (E_0 = ground state energy). Since $E_0 = E_v [n_0]$, where n_0 is the true ground-state electron density, the true ground-state electron density minimizes the energy functional $E_v [n_{tr}]$, just as the true normalized ground-state wave function minimizes the eigenvalue in a Schrödinger equation.[10].

Consider that n_{tr} satisfies the above stated conditions, $\int n_{tr}(r)dr$ = N and $n_{tr}(r) \geq 0$ for all r. The Hohenberg-Kohn theorem states that n_{tr} uniquely determines the external potential v_{tr} and this in turn determines the trial wave function ,Ψ_{tr} that corresponds to n_{tr} . Now the energy corresponding to this wave function Ψ_{tr} is,

$$E = \langle \Psi_{tr} | H | \Psi_{tr} \rangle \tag{2.16}$$

$$= \langle \Psi_{tr} | T + U + \sum_i v_i(r) | \Psi_{tr} \rangle \tag{2.17}$$

$$E_0 = E_v[n_0] \qquad (2.18)$$

Since the kinetic and interaction energies are functionals of the electron density and using the ground state wave function Ψ_0 , we have,

$$T[n_{tr}] + U[n_{tr}] + \int n_{tr}v(r)dr \geq E_v[n_0] \qquad (2.19)$$

$$E_v[n_{tr}] \geq E_v[n_0] \qquad (2.20)$$

This proves that any trial electron density can not give rise a lower ground-state energy than the true ground-state electron density.

2.5   The Kohn-Sham equations

The Hohenberg-Kohn theorem tells us about the the ground state properties of a system given the ground state density n(r). However, it does not address the fact about how to find the ground state energy E_0 from the ground state density $n_0(r)$ or how to find $n_0(r)$ without first finding the wave function. Kohn and Sham addressed this problem and made the practical application of DFT possible.[11].

In this formulation, the system of interacting electrons is mapped on to a system of non interacting particles having the same electronic density $n_0(r)$ as that of the interacting one. For such a system the ground state density can be represented as;

$$n(r) = 2\sum_{i=1}^{N/2} |\psi_i(r)|^2 \qquad (2.21)$$

where $\psi_i(r)$ is the Kohn-Sham orbital

N is the total number of electrons.

The KS orbitals are the solutions of the Schrödinger equation:

$$(-(\hbar^2/2m)\nabla^2 + V_{KS}(r))\psi_i(r) = \epsilon_i\psi_i(r) \qquad (2.22)$$

Where V_{KS} is the Kohn-Sham potential. It is the effective external potential in which

the non-interacting electrons move.

Now, let us define a term ΔT as,

$$\Delta T[n] = T[n] - T_s[n] \tag{2.23}$$

which is the difference between the K.E. of the real system and the system of non-interacting electrons which has the same density as the real system.

Also;

$$\Delta U[n] = U[n] - \frac{1}{2} \int \int \frac{n(r_1)n(r_2)}{|r_1 - r_2|} dr_1 dr_2 \tag{2.24}$$

Hence, the total energy functional becomes;

$$E_0 = E_\nu = \int n(r)\nu(r)d(r) + T_s[n] + \frac{1}{2} \int \int \frac{n(r_1)n(r_2)}{|r_1 - r_2|} dr_1 dr_2 + \Delta T[n] + \Delta U[n] \tag{2.25}$$

Here the functionals $\Delta T[n]$ and $\Delta U[n]$ together define the exchange correlation function.

Hence, the total energy functional now has the form;

$$E_0 = E_\nu = \int n(r)\nu(r)d(r) + T_s[n] + \frac{1}{2} \int \int \frac{n(r_1)n(r_2)}{|r_1 - r_2|} dr_1 dr_2 + E_{XC} \tag{2.26}$$

Here the first three are fairly easy to calculate if the ground state density is known and contributes mostly to the ground state energy. The exchange correlation term however is very difficult to calculate and finding an accurate solution for it has been one of the greatest challenge in DFT.

2.6   Self consistent nature of Kohn-Sham equations

Given the constraint that the total number of electrons in the system are constant, the ground state density can be found by varying the electron density so as to minimize the energy functional. This is the basis of Hohenberg-Kohn variational principle. Hence, the energy functional for the system of interacting particles is given by the equation (2.15). This can be minimized using Lagrange multiplier method. So,with the constraint that total

number of electrons are constant, the Euler-Lagrange equation becomes

$$\delta E_\nu[n(r)] = \int \delta n(r) \left(v_{eff}(r) + \frac{\delta}{\delta n(r)} T_s[n(r)] - \epsilon \right) dr = 0$$

(2.27)

where

$$v_{eff}(r) = v_{ext}(r) + \int \frac{n(r_2)}{|r_1 - r_2|} dr_2 + v_{xc}(r)$$

(2.28)

and

$$v_{xc}(r) = \frac{\delta}{\delta n(r)} E_{xc}[n(r)] \tag{2.29}$$

This is the exchange-correlation potential. Now, the Eq.(2.27) has the similar form as the equation for system of non interacting particles with an effective potential v_{eff} (which is also called as Kohn-Sham potential). The minimum of the electron density n(r) can be found by solving single particle Schrödinger equation

$$[-\frac{\hbar^2}{2m} \nabla^2 + V_{eff}(r)]\psi_i(r) = \epsilon_i \psi_i(r) \tag{2.30}$$

with

$$n(r) = 2 \sum_{i=1}^{N/2} |\psi_i(r)|^2 \tag{2.31}$$

and effective potential given by (2.28). Equations (2.30), (2.31) and (2.28) together form the set of self- consistent Kohn-Sham equations.[12]. Self-consistency implies that we can start from an initial guess for the ground state density $n(r)$ and construct the Kohn-Sham potential from Eq. 17. Then the single particle Schrödinger equations is solved and a new density, which should be same as initial $n(r)$,is calculated. If not within tolerance limit, the

new density is fed back as an initial guess and the entire process is performed reiteratively until the final density falls below tolerance limits.

2.7   Periodic Supercells

Previously it was shown that the many-body problem of the interacting electron can be mapped into a single body problem consisting of non-interacting electrons. However, there still remains the problem of handling an infinite number of non-interacting electrons moving under the influence of infinite number of nuclei or ions. In doing so, two hurdles must be overcome; there must be a wavefunction for each of the infinite number of electrons and the basis set required to expand each such wavefunction is infinite.

These difficulties can be overcome by using periodic boundary condition and applying Bloch's theorem for electronic wavefunctions.[13].

Bloch's Theorem

" Bloch's theorem states that in a periodic solid each electronic wave function can be written as the product of a cell-periodic part and a wavelike part"[13].

$$\psi_i(r) = exp[ik \cdot r] f_i(r) \tag{2.32}$$

The cell periodic part can be further expanded;

$$f_i(r) = \sum_G c_{i,G} exp[iG \cdot r] \tag{2.33}$$

Where G the reciprocal lattice vector is defined as; $G \cdot l = 2\pi m$, for all l where l is a lattice vector of the crystal and m is an integer. Now, each electron wave function can be written as a sum of plane waves;

$$f_i(r) = \sum_G c_{i,G} exp[i(K + G) \cdot r] \tag{2.34}$$

14

k point sampling

The boundary condition that applies to the bulk solid determines the set of k point for which the electronic states are allowed. The density of allowed k points is proportional to the volume of the solid. The Bloch theorem helps in changing the problem of calculating an infinite number of wave functions to one which requires calculating a finite number of electronic wavefunctions at an infinite number of k points. The occupied state at each k point contributes to the electronic potential in the bulk solid. Hence, infinite number of calculations are needed to compute this potential. However we use a finite number of k points to calculate the electronic potential and the total energy of the solid since it is not possible to do calculations for infinite number of k points.

The magnitude of any error in the total energy due to the insufficiency of the k point sampling can be reduced by using a denser k point set. As the density of the k point increases the computed total energy converges and the error approaches zero.

Smearing method

There are several problems associated with metallic system. Brillouin-zone integrals over functions are discontinues at Fermi level due to partially filled band. Also, high Fourier components and hence, large number of k- points are required. This difficulty is overcome by introducing an artificial smearing to the problem. There are several schemes to achieve smearing, each having its own advantages and disadvantages. In order to improve convergence with number of k-points, the step function is replaced by a smoother function. Few of those various schemes are Gaussian, Fermi-Dirac, Methfessel-Paxton, Marzari-Vanderbilt.[14].

2.8 Exchange-Correlation energy: LDA and GGA

2.8.1 Local Density Approximation

In the Kohn-Sham formulation, the Schrödinger Equation takes up the form of N-single body equations which is given as follows:

$$(-\frac{1}{2}\nabla^2 + \nu_{KS}(r))\psi_i(r) \qquad (2.35)$$

whereas Kohn-Sham potential is given as

$$\nu_{KS}(r) = \nu_{ext}(r) + \nu_H(r) + \nu_{xc}(r). \qquad (2.36)$$

The last term depends on the electron-electron interaction and is called the exchange-correlation potential,

$$\nu_{xc}(r) = \frac{\delta E_{xc}[n(r)]}{\delta n(r)} \qquad (2.37)$$

The equation presented above is complete with no approximations made so far. However, the functional form of the exchange-correlation energy is not known and hence approximations are necessary to get the estimate of the contribution of this term. In 1965, Kohn and Sham described a simplest method to estimate exchange-correlation energy of an electronic system and is called as the Local density approximation (LDA).[13]. The exchange-correlation energy at any point **r** in the electron gas is assumed to be same as that of homogeneous electron gas having equal electron density as that of the system in consideration. Therefore,

$$E_{xc}[n(r)] = \int \varepsilon_{xc}(r)n(r)d^3r \qquad (2.38)$$

and the potential becomes

$$\frac{\delta E_{XC}[n(r)]}{\delta n(r)} = \frac{\partial[n(r)]\varepsilon_{XC}(r)}{\partial n(r)} \qquad (2.39)$$

with $\varepsilon_{XC}(r) = \varepsilon_{XC}^{hom}[n(r)]$

Kohn-Sham, Perdew- Zunger, Vosko and others have given different ways to parametrize the exchange-correlation energy of a homogeneous electron gas [15], all of which give similar

result. The most common is that of Perdew and Zunger, who gave simple analytic form of the former based on the highly accurate quantum-Monto Carlo techniques, founded by Ceperley and Alder.[16].

The local-density approximation assumes that the exchange-correlation energy is completely local and it neglects the corrections to the same due to inhomogeneities in the electron density around the point r. In spite of this crude approximation. the calculations using LDA so far have been remarkably successful. Further studies have shown that this success is related to the fact that the LDA gives the correct sum rule for exchange correlation hole.

2.8.2 Generalized Gradient Approximation

Generalized Gradient Approximation is the simplest approximation of inhomogeneity to the local-density approximation. This is a semi-local method in which the energy of the true density is approximated by the density which is a function of a constant local density and a local gradient of the density.[17]. The GGA exchange-correlation energy functional can be written as

$$E_{xc}^{GGA}[n(r)] = \int n(r) \varepsilon_{xc}^{hom}[n(r)] F_{xc}[n(r), \nabla n(r)] dr \tag{2.40}$$

The enhancement factor F_{xc} is a function of electron density at a point r and of the gradient of local density $\nabla n(r)$. Like LDA, there are many possible parametrizations of GGA and each one leads to a different enhancement factor. Initially,the acceptance of GGA has been rather slow due to mixed results. GGA performed better for atomic energies and binding energies than LDA at relatively modest computational cost. Especially, in case of Hydrogen, GGA provided a very good description of the hydrogen bonds.

Local density as well as Generalized Gradient approximations are used extensively in the study of electronic and magnetic interactions of semiconductor materials. However, there are several problems involved in the estimation of band gap values which may result in incorrect predictions of the properties of such materials.

2.9 Hellmann-Feynmann Forces

Hellman-Feynmann theorem relates the derivative of the total energy with respect to some parameter, to the expectation value of the derivative of the Hamiltonian with respect to the same parameter.[18]. This allows one to calculate the forces on the atom once the ground state density of the electron is calculated through self-consistent iterations. In a system of atoms, the force on the $\imath$ th atoms is given by,

$$\bar{F}_\imath = -\frac{\delta E}{\delta \bar{R}_\imath} \tag{2.41}$$

The ground state energy is given by $E_e = \langle\Psi|\hat{H}|\Psi\rangle$ As atoms change their positions, the wave function is changed in such a way that the eigenstates will correspond to the new position of the atom if the value of the Kohn-Sham energy functional is to remain meaningful. These changes contribute to the force on the atom. This can be further explained as follows :

Substituting ground state energy equation into (2.41), we get

$$\bar{F}_\imath = -\langle\frac{\delta\Psi}{\delta\bar{R}_\imath}|\hat{H}|\Psi\rangle - \langle\Psi|\frac{\delta\hat{H}}{\delta\bar{R}_\imath}|\Psi\rangle - \langle\Psi|\hat{H}|\frac{\delta\Psi}{\delta\bar{R}_\imath}\rangle \tag{2.42}$$

Rearranging the terms,

$$\bar{F}_\imath = -E[\langle\frac{\delta\Psi}{\delta\bar{R}_\imath}|\Psi\rangle + \langle\Psi|\frac{\delta\Psi}{\delta\bar{R}_\imath}\rangle] - \langle\Psi|\frac{\delta\bar{H}}{\delta\bar{R}_\imath}|\Psi\rangle = E\frac{\delta}{\delta\bar{R}_\imath}\langle\Psi|\Psi\rangle - \langle\Psi|\frac{\delta\hat{H}}{\delta\bar{R}_\imath}\Psi\rangle$$

$$= \text{-}\langle\Psi|\frac{\delta\hat{H}}{\delta R_\imath}|\Psi\rangle = -\frac{\delta E}{\delta R_\imath} \tag{2.43}$$

This last equation explains that the forces can be computed just by the change in the Hamiltonian operator. This also shows that the partial derivative of the Kohn-Sham energy with respect to the position of an atom gives the real physical force on the atom. In practical problems, it is difficult to compute energy derivatives numerically. However, the Hellmann-Feynmann force can be computed efficiently, which is negative of that derivative.

2.10   Plane-Wave Basis and Pseudo-potential

Once the periodic boundary conditions (PBC) are implemented in the Kohn-Sham equations, the equation becomes;

$$\left(-\frac{\hbar^2}{2m}\nabla^2 + V_{KS}(r)\right)\psi_{nk}(r) = \epsilon_{nk}\psi_{nk}(r) \tag{2.44}$$

where, n is the band index and **k** is the crystal momentum.

Now, V_{KS} is:

$$V_{KS}(r) = V_{ion}(r) + \int dr' \frac{n(r')}{|r - r'|} + V_{xc}(r) \tag{2.45}$$

and the electron density is given by,

$$n(r) = \sum_{n\mathbf{k}} |\psi_{n\mathbf{k}}|^2 \tag{2.46}$$

Given an explicit V_{KS}, we now have the practical issue of solving these coupled equations efficiently.

Plane-Wave basis

Theoretically, in order to solve the Kohn-Sham equations, one needs to choose a basis to expand the wavefunction $\psi_{n\mathbf{k}}$ and then to truncate the basis so that calculation time is finite.[19]. The most natural choice of basis is the plane wave basis, because of the periodic part in the Bloch state $\psi_{n\mathbf{k}}$, which can be expanded in a Fourier series.

$$\psi_{n\mathbf{k}}(\mathbf{r}) = e^{i\mathbf{k.r}}u_{n\mathbf{k}}(\mathbf{r}) = e^{i\mathbf{k.r}}\sum_{\mathbf{G}} c_{n\mathbf{k}}(\mathbf{G})\frac{e^{i\mathbf{k.r}}}{\sqrt{\Omega}}$$

(2.47)

Ω is the volume of the unit cell.

By inserting equation (2.47) in the Kohn-Sham equation (2.44), we find that $c_{n\mathbf{k}}(\mathbf{G})$ satisfy:

$$\frac{|K+G|^2}{2}c_{n\mathbf{k}}(\mathbf{G}) + \sum_{G'} V'_{KS}(\mathbf{G}-\mathbf{G}')c_{n\mathbf{k}}(\mathbf{G}') = \epsilon_{n\mathbf{k}}c_{n\mathbf{k}}(\mathbf{G}) \tag{2.48}$$

Where V'_{KS} is the Fourier transform of V_{KS}.

To get a finite number of $(\mathbf{G})$ basis, we need to set-up a cutoff,

$$\frac{|\mathbf{K}+\mathbf{G}|^2}{2} \leq E_{cut} \tag{2.49}$$

By equation (2.48) and (2.49), though in principle any level of accuracy can be reached by increasing the E_{cut}, in practice this method is futile. The reason being that in solids the core electrons are tightly bound to the nuclei. Their wavefunction changes rapidly in the core region and decay away quickly. In order to describe these wavefunction accurately we need many plane waves (large G) to expand these functions. However, these core electrons are so tightly bound to the nuclei that they seldom take part in bonding of solids or molecules. Therefore, by using plane wave basis we waste a lot of effort to describe these electrons which are not of that importance to us.

Pseudo-potential

As explained in the previous section, the bonding properties of the material is mostly dependent on the valence electrons rather than the core electrons. Therefore, as a good approximation we treat core electrons to be immobile and stuck to the nucleus, the so called frozen-core approximation.

Even with the frozen core approximation, the numerical calculation which involve valence electrons could still be very expensive. The reason is that in order to be orthogonal to the wave function of the core electrons and other valence electrons, the wave functions of valence electrons must have nodes in the core region, which leads to rapid oscillations. Describing rapid oscillations of wave functions in the core region needs many plane wave basis, which is the hindrance for realistic computation. To find a way around this obstacle, we need to notice that most bonding takes place in the interstitial region rather than in the core region.

If we can construct an artificial potential which accurately reproduces the wave functions of valence electrons in the interstitial region but replaces the oscillating part of wave functions by a smooth one.[13]. Numerous tests show that by implementing the pseudo-potential in realistic simulations not only reduces the computation cost significantly but also provides good description of chemical bonding.

There are quite a few different algorithms concerning the generation of a pseudo- potential, which can be found in the literature [13].

Chapter 3

Results and Discussions

3.1 Computational Method

Our calculations are performed using density functional theory (DFT) with plane wave basis set with the code PWscf in the Quantum-ESPRESSO package.[22]. We employ the generalized gradiant approximation (GGA) based parametrization by Purdew, Burke and Ernzenhof (PBE)[23] and ultrasoft pseudo-potential. The plane wave basis energy cutoff and charge cutoff are 35 Ry and 360 Ry respectively. We use Marzari-Vanderbilt smearing width of 0.01 Ry. The k-grid sampling of the Brillouin zone is done with the $12 \times 12 \times 1$[24] k-point mesh. Through our calculations we have obtained the lattice parameter of the Ni bulk to be 3.52 Å (and hence the lattice parameter of Ni(111) is 2.49 Å) and that of graphene to be 2.46 Å which are in good agreement with the earlier reported values [25].

Our system is modeled with a symmetric slab of 6 Ni(111) layers. The bottom three layers are kept fixed while other three are relaxed till the forces are converged to a value within 0.002 eV/ Å. In all our calculations, the interfaces are along the (001) direction so that the z axis is perpendicular to the interface. The x and y directions of the simulation cell are subject to periodic boundary conditions.

The fixed bottom layer is coated with Cu atoms to quench the artificial magnetization. To avoid the interaction between the periodic images, a vacuum of about 15 Å is used. In practice, when graphene is grown on a substrate, the graphene sheet is strained by the substrate potential. The amount of strain depends on the degree of lattice mismatch. In the

case of Ni(111) surface, there is an almost perfect lattice matching with graphene. Hence the graphene sheet is expected to grow pseudomorphically on the Ni substrate. Therefore, to study the interactions of graphene sheet with the Ni substrate, both the graphene and Ni substrate are kept at the Ni(111) lattice parameter of 2.49 Å. Dispersive interactions play an important role in graphene-transition metal interfaces, which is not taken into account by conventional PBE exchange correlation functional. Therefore, we have included an empirical Van der Waals (vdW) correction to account for the dispersive interactions. However, we note that this is an empirical correction to the total energy and it does not affect the magnetic couplings of the system.

3.2   Oxygen adsorption on Ni(111) slab

The adsorption of O on Ni(111) slab was calculated for the 1ML (mono-layer) uniform coverage. i.e. the ratio of the number of oxygen atoms to the number of surface Ni atoms in the unit cell was maintained at 1:1. The binding energy of oxygen on Ni slab is calculated using the equation (3.1).

$$\Delta E_{Ni-O} = E_{Ni+O} - E_{Ni} - \frac{1}{2}E_O \tag{3.1}$$

Where, E_{Ni+O} is the energy of the configuration considered.

E_{Ni} is the energy of the symmetric Ni-slab.

and, E_O is the energy of the oxygen molecule.

It is well known that oxygen prefers to occupy one of the hollow sites (hcp and fcc site).[ref]. Hence, calculations were carried out for the two hollow sites and it was found that oxygen atoms prefer to occupy fcc site over the hcp hollow site [fig 3.1(a)]. The binding energy for the fcc configuration was found to be -1.42 eV/O atom while the binding energy of the hcp was -1.27 eV/O atom. [26]. The Ni-O inter-planar distance for the fcc configuration was calculated to be 1.14 Å.

Similar calculations were carried out for 0.5 and 0.25 ML coverage of O on Ni(111) slab using a (2 × 2) super cell. In both the cases, the oxygen atom occupying the fcc-hollow site was most favored energetically. For the 0.5 ML coverage the binding energy per oxygen

<center>(a)   (b)</center>
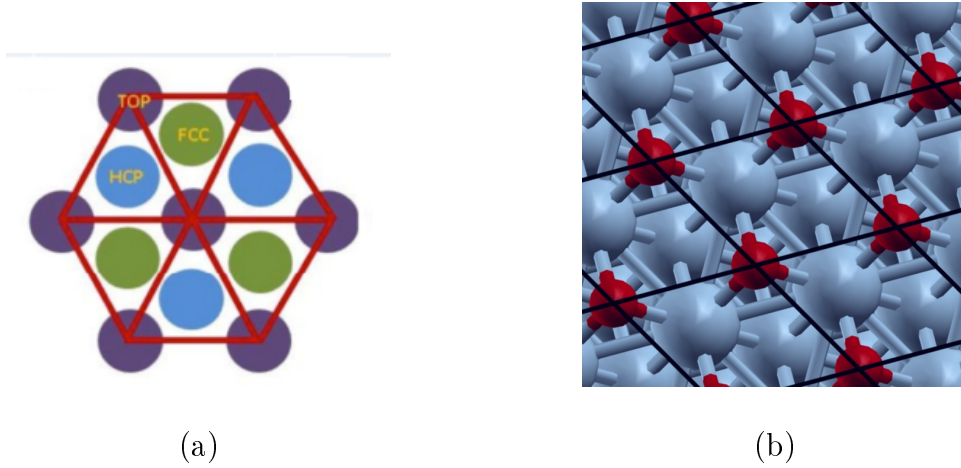
Figure 3.1: (a) A schematic diagram depicting the hcp, fcc and top site. (b) Top view of the most stable Ni(111)-O configuration (O on the fcc hollow site). Here the O and Ni atoms are denoted by small red and large blue spheres respectively.

atom of the fcc and hcp case are found to be -2.40 and -2.27 eV respectively while for the 0.25 ML coverage it is -2.87 eV and -2.75 eV respectively. [26].

3.2.1   Addition of Graphene on Ni(111)-O

The carbon atoms on the graphene sheet has different possible sites on the 1 ML coverage which it can potentially occupy. We have considered six such configurations, which are given below.

(a)**top − fcc**:One C atom is placed directly above the surface Ni atom and the other C atom is on the void fcc site

(b)**top − hcp**: One C atom is placed directly above the surface Ni atom and the other C atom is on the void hcp site

(c)**hcp − fcc**: One C atom is on the void hcp site and the other on void fcc site

(d)**bridge − hcp**: One C atom is in the middle of the adjacent hcp and top site and the other C atom is in the middle of adjacent hcp and fcc site

(e)**bridge − top**: One C atom is in the middle of the adjacent top and hcp site and the other C atom is in the middle of adjacent top and fcc site

(f)**bridge − fcc**: One C atom is in the middle of the adjacent fcc and hcp site and the other C atom is in the middle of adjacent fcc and top site

<center>24</center>

Here, the binding energy of the graphene sheet is calculated using the equation (3.2).

$$\Delta E_{Gr} = (E_{Ni+O+C} - E_{Ni+O} - E_{Gr})/2 \qquad (3.2)$$

Where, E_{Ni+O+C} is the energy of the configuration considered.

E_{Ni+O} is the energy of the fcc-O configuration.

and, E_{Gr} is the energy of the free standing graphene.

Table 3.1: The table shows the values of binding energies for different configurations of graphene on Ni(111)-O surface.

Initial configuration w.r.t Ni surface	Final configuration w.r.t Ni surface	Binding energy ΔE_{Gr} (eV/C)	(C-O interplanar distance (Å)
Top-fcc	Top-fcc	-0.095	2.86
Top-hcp	Top-hcp	-0.100	2.81
Hcp-fcc	Hcp-fcc	-0.090	2.86
Bridge-top	Bridge-top	-0.095	2.86
Bridge-hcp	Bridge-hcp	-0.030	3.42
Bridge-fcc	Bridge-fcc	-0.120	2.85

From the table (3.1) it is observed that, out of all the possible configuration of carbon atoms, the bridge-fcc configuration is found to be the most stable with a binding energy of -0.120 eV/C atom and the C-O inter-planar distance in this case is observed to be 2.85 Å. [fig (3.2).]

(a)   (b)
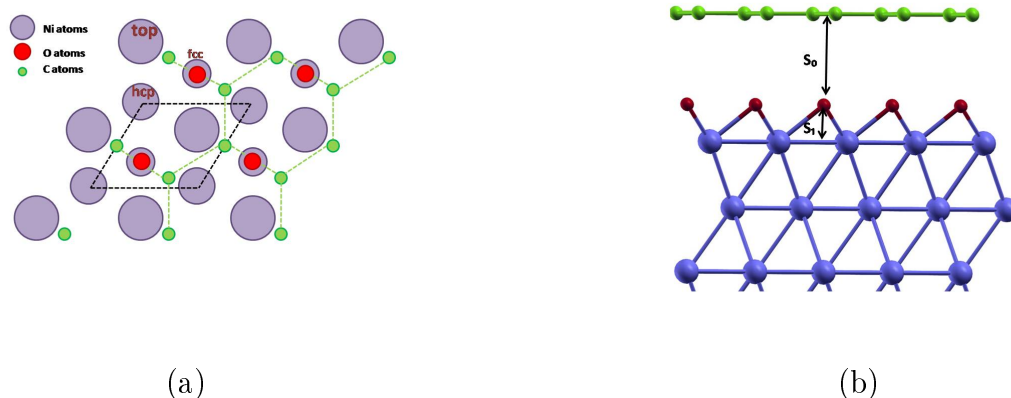
Figure 3.2: (a) A schematic diagram of bridge-fcc configuration. (b) Side-view of bridge-fcc configuration

Having obtained the most stable configuration for graphene on Ni(111)-O, the magnetization density and projected density of states(PDOS) plots were obtained. (fig 3.3(a)). The magnetization density plot (fig 3.3(b)) shows that there is no induced magnetic moment on graphene which is in contrast with what was observed without the intercalation of the O-spacer layer between Ni(111) and graphene. In that case graphene had an induced magnetic moment of $0.01\mu_B$.[27]

When the oxygen intercalated layer is not present between the Ni and graphene, there are interactions between surface Ni atoms and carbon atoms resulting in an induced magnetic moment on graphene. Upon intercalation, the interactions between the Ni and carbon atoms are quenched resulting in zero net magnetic moment on graphene.

The PDOS plot [fig 3.3(a)] shows that there is a weak overlap of C-$2p$ and Ni-$3d$- states. The C-p states show negligible exchange splitting.

(a)   (b)
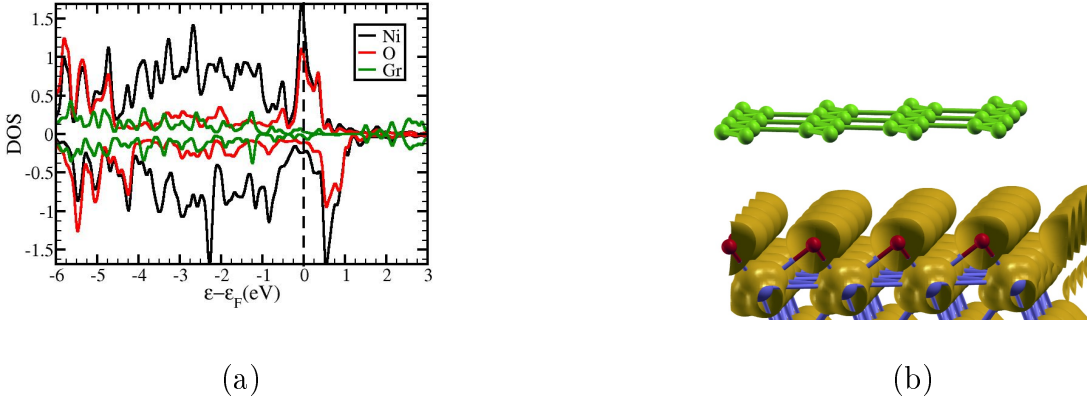
Figure 3.3: (a) PDOS plot indicating zero overlap of $2p$-C and $3d$-Ni states and negligible exchange splitting. (b) Magnetic density plot has no iso-surface on the C-atoms indicating no induced magnetic moment on graphene.

We have also looked into the electronic band structure plots of graphene on Ni-O surface.(fig 3.4) The band structure plot reveals that the Dirac cone is still observed at the K point of the Brillouin zone (BZ) as seen in the free-standing graphene, only in this case it is slightly shifted above the Fermi level. This suggests that the graphene is not completely free from the surface-Ni atoms. Long range Van-der-Waal interactions exist between the graphene and the surface-Ni which results in the shifting of the Dirac-cone above the Fermi
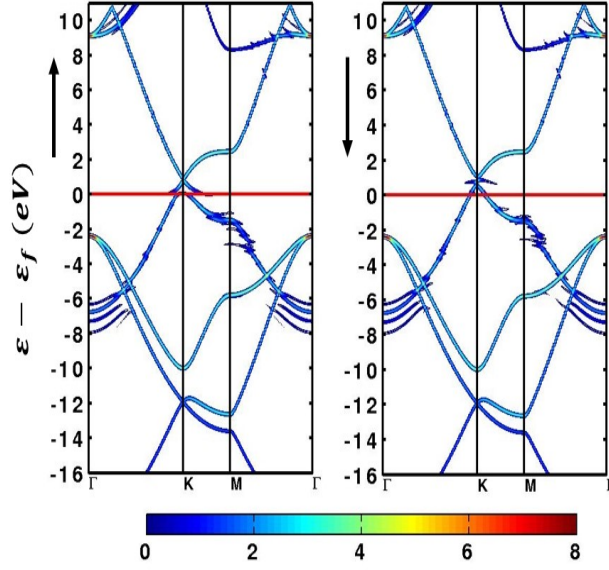
level.

Figure 3.4: The K-point resolved projected density of states plot (KPDOS) or the band-structure plot for the bridge-fcc configuration shows that the Dirac-cone is shifted slightly above the fermi energy indicating the presence of weak long range dispersive interaction between graphene and Ni(111)-O surface.

3.2.2   Semi-hydrogenation of graphene on Ni(111)-O Surface

The graphene sheet on the Ni(111)-O slab is now semi-hydrogenated(graphone). We have studied this in detail for three different coverages of O atoms .i.e. 1ML, 0.5ML and 0.25ML coverages. The binding energy of graphone on Ni-O for all the three cases are calculated using the equation (3.3).

$$\Delta E_{GrH} = E_{Ni+O+GrH} - E_{Ni+O} - E_{GrH} \tag{3.3}$$

Where, $\Delta E_{Ni+O+GrH}$ is the binding energy of graphone on Ni-O, $E_{Ni+O+GrH}$ is the ground state energy of the particular configuration considered and E_{GrH} is the energy of the free standing graphone.

1ML coverage of O atoms

For the 1ML coverage the most stable configuration of O on Ni slab was the fcc-configuration
as seen previously. The graphene sheet on the Ni(111)-O slab is now semi-hydrogenated(graphone).
There can be twelve such configurations depending on the position of the H atoms on
graphene. Table 3.2 summarizes the results obtained.

Table 3.2: The table shows the values of binding energies for different configurations of graphone
on Ni(111)-O surface. ΔE_{GrH} is the binding energy of graphone calculated by eq (3.3).

Initial configuration w.r.t Ni surface	Initial position of H atom	Final configuration w.r.t Ni surface	Final position of H atom	ΔE_{GrH} (eV)/C	C-O inter-planar distance (Å)
Top-hcp	top	Top-hcp	Top	-0.36	1.89
Top-hcp	hcp	Top-hcp	Hcp	-0.23	2.18
Top-fcc	top	Top-fcc	Top	-1.29	1.40
Hcp-fcc	hcp	Hcp-fcc	Hcp	-1.15	1.39
Hcp-fcc	fcc	Hcp-fcc	Fcc	-0.29	2.37
Bridge-hcp	Hcp-top	Bridge-hcp	Hcp-top	1.45	2.49
Bridge-hcp	Hcp-fcc	Hcp-fcc	Hcp	-1.16	1.40
Bridge-fcc	Fcc-top	Hcp-fcc	Hcp	-1.17	1.40
Bridge-fcc	Fcc-hcp	Top-fcc	Top	-1.29	1.40

From the table 3.2 it can be seen that the most stable configuration is the top-fcc con-
figuration [fig.3.5(a)]. .i.e. one C atom on O (fcc) and the other C on top site with H atom.
Figure 3.5(b) depicts the magnetization density plot for the most stable configuration, where
yellow colored iso-surface is seen on the surface Ni atoms which shows the net spin-up mag-
netic moment on the surface Ni atoms. It is indeed seen that the magnetic moment of surface
Ni atom increases from 0.19 to 1.00 μ_B, a mammoth five-fold increase.

To gather more insight into this we performed the charge transfer analysis for the system.
Figures 3.6(a) and 3.6(b) shows the result of our charge transfer analysis, where the blue
iso-surfaces indicate the regions of charge depletion and red iso-surface show the regions of
charge accumulation. Thus we see that the spin up electrons from fcc-C are transferred to Ni
atoms and spin-down electrons are transferred from surface Ni to fcc-C. This charge transfer
is mediated via the oxygen atoms.

To understand the transfer of charges in this particular fashion, we had plotted the
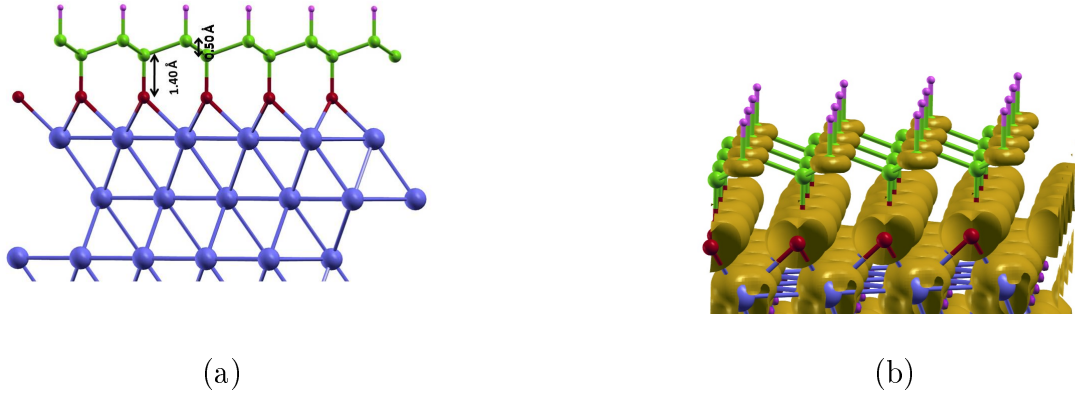
| (a) | (b) |

Figure 3.5: (a) Most stable configuration upon hydrogenation (top-fcc) (b) Magnetic density plot showing yellow iso-surface on the surface Ni atoms indicating net spin-up magnetic moment on surface Ni atoms .

projected density of state plots (PDOS) for the non-interacting (graphone on Ni-O) and the interacting cases. [fig 3.7(a) and 3.7(b)]. What we had observed is that for the spin-up case, the states corresponding to Ni-O peaks at the Fermi energy indicating that the Ni-O states are partially filled. The C(without H) states are completely filled. The Fermi level of the slab and HOMO of graphone are very close in energy and hence when we place graphone on Ni-O the up-electrons of the C atom(without H) moves to the half filled state of Ni-O. Similarly, after accepting the electrons from the C atom the Ni-O states are occupied and move below Fermi energy. The down-spin electrons move in a reverse fashion to the up-spin electrons. Hence, due to the combined effect of the movement of charges there is a huge increase in the magnetic moment of surface Ni atoms.

0.5ML coverage of O atoms

For the 0.5 ML coverage a (2×2) super cell was used and the Brillouin Zone (BZ) integration is carried out with Monkhorst-Pack k-point grid of $6 \times 6 \times 1$. All other parameters are kept same as 1ML case.
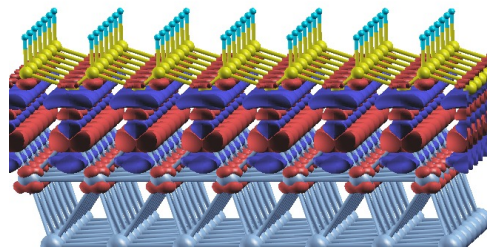
All different configurations for graphone on this case were considered. The hcp-fcc configuration (with H on the hcp site) is found to be the most stable with a binding energy of -1.72 eV/C atom. It is seen from fig 3.8(b) that there are three different types of C atoms
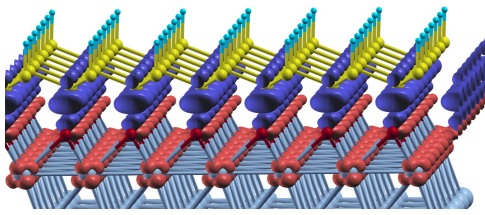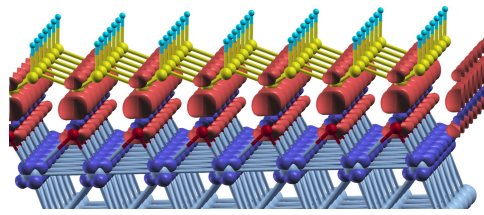
Figure 3.6: (a) Charge density transfer plot for spin-up and (b) spin-down electrons. (c) Total charge transfer plot. The red color shows the accumulation of charge while the blue color depicts the depletion of charge.
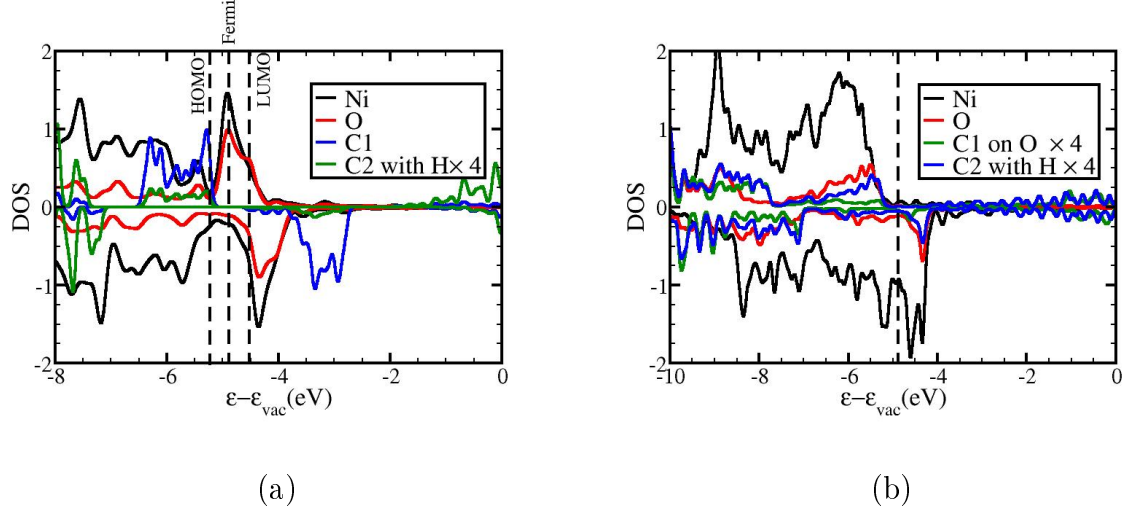
Figure 3.7: (a) PDOS plot for the non interacting system. Here the HOMO and LUMO of the free-standing graphone and the Fermi energy of the Ni-O system is shown. (b) PDOS for the interacting system. The electrons from the filled $2p$-C1 spin-up state moves to $2p$-O and $3d$-Ni states making them fully occupied.
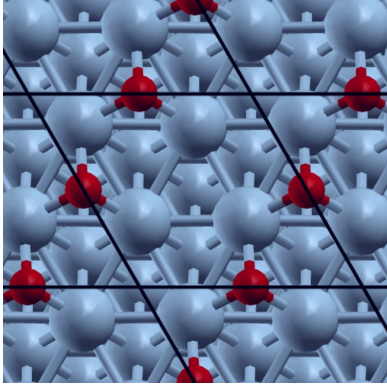
present in this configuration, one which binds to oxygen, one which binds to hydrogen and one which is not bound to H or O. The three C atoms in this case are separated by a distance of 1.41 Å, 1.91 Å and 1.60 Å respectively from the oxygen layer.

The study of the magnetization density plot [fig 3.9(a)] for this case shows yellow iso-surfaces on surface Ni atoms and the carbon atom which are not bound to H or O atoms indicating that the magnetic moment of both these atoms are paralelly aligned. It is indeed observed that the surface Ni atoms have a magnetic moment of 0.72 μ_B and that of graphene is 0.31 μ_B, where the contribution of the moments mainly come from the C atom not bound to H or O. The magnetic moment of C which does not bind to H or O is found to be 0.65 μ_B.
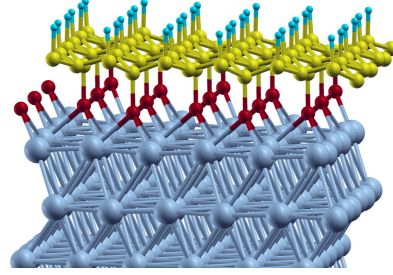
The carbon which does not bind to O or H has an increased magnetic moment as its lone pair is free and hence it contributes in an increased magnetic moment.[fig 3.9(b)]

0.25 ML coverage of oxygen atom

For 0.25 ML coverage of oxygen atom on Ni(111), the hcp-fcc configuration (with H on hcp carbon) was found to be most stable. The binding energy of graphone on Ni-O surface was

(a)   (b)

Figure 3.8: (a) The Ni-O slab for the 0.5ML coverage of oxygen where O occupy the fcc site. (b) The most stable Ni+O+GrH configuration for the 0.5ML coverage of oxygen. There are three different types of C atoms present in this configuration, one which binds to oxygen, one which binds to hydrogen and one which is not bound to H or O.

found to be -1.52 eV/C atom.[eqn 3.3].

It can be seen from the fig 3.10(b) that the hcp-fcc configuration consists of three different types of C atom viz. one which is bound to the H atom, one bound to the O atoms and another bound to the Ni atom. Another peculiar thing which is observed is the buckling in the surface Ni atoms. One of the Ni atom is slightly shifted above the others.

The magnetization density plot [fig 3.11(a)] shows yellow iso-surface on the surface Ni atoms and pink iso-surface on the shifted Ni atoms indicating that the magnetic moments of these two Ni atoms are anti-parallely aligned.

The average magnetic moment of surface Ni atoms and the shifted atom is found to be $0.62\mu_B$ while graphene has almost zero induced magnetic moment.

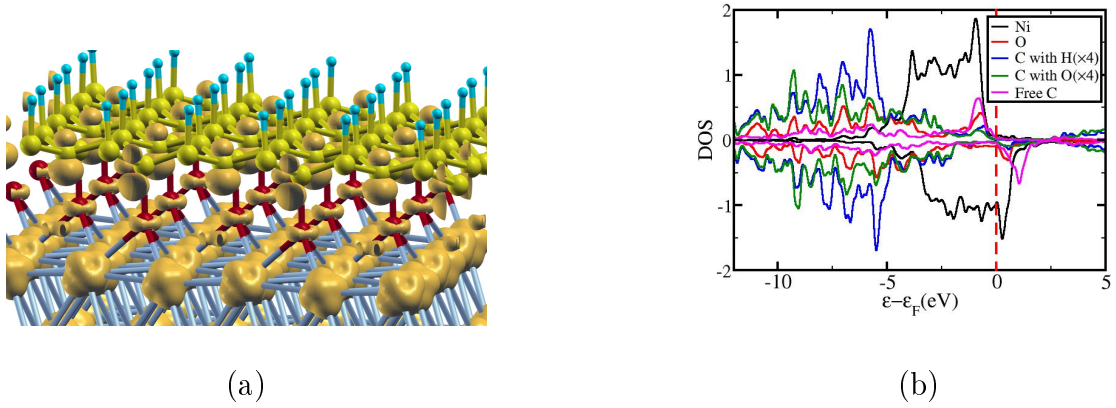|	
(a)	(b)

Figure 3.9: (a) The magnetization density plot for the hcp-fcc configuration showing yellow iso-surfaces on surface Ni atoms and the carbon atom which is not bound to H or O atoms indicating that the magnetic moment of both these atoms are paralelly aligned.(b) Projected density of states (PDOS) for this case.
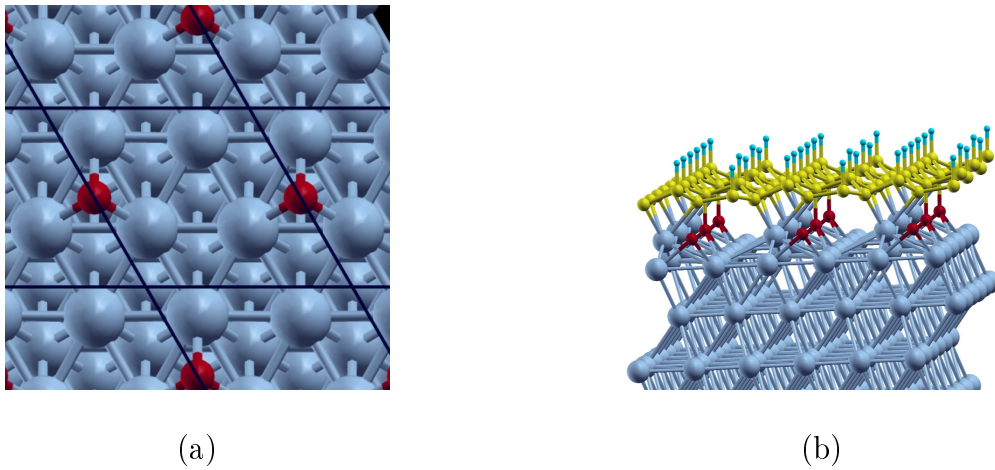

(a)	(b)

Figure 3.10: (a) The Ni-O slab for the 0.25ML coverage of oxygen where O occupy the fcc site. Here we can see that for every four Ni atoms in the unit cell there is one oxygen atom.(b) The most stable Ni+O+GrH configuration for the 0.25ML coverage of oxygen. There are three different types of C atoms present in this configuration, one which binds to oxygen, one which binds to hydrogen and one which is bound to Ni atom.
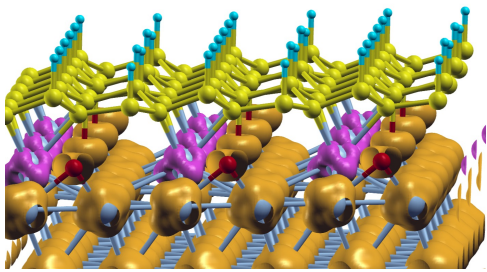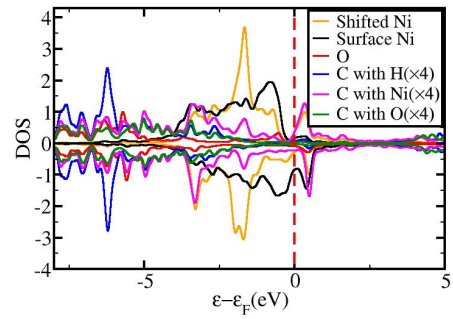
Figure 3.11: (a) The magnetization density plot for the hcp-fcc configuration showing yellow iso-surfaces on surface Ni atoms and pink iso-surface in the shifted Ni atoms indicating that the magnetic moment of both these atoms are anti-paralelly aligned.(b) Projected density of states (PDOS) for this case.

Chapter 4

Conclusion

We have studied in detail the electronic and magnetic properties of graphene and graphone supported on oxygen adsorbed Ni(111) surface. Introduction of the oxygen mono-layer spacer decouples the pristine graphene sheet from Ni(111) substrate making it quasi-free standing. The Dirac cone again appears in the bandstructure at K point of the Brillouin zone but only slightly shifted above the Fermi energy because of the weak interactions between the graphene sheet and the oxygen adsorbed Ni(111) substrate. The semi-hydrogenated graphene (graphone) sheet binds more strongly to the oxygen adsorbed on Ni(111) substrate . The magnetic moments on the carbon atoms of graphone are completely quenched due to the sigma bond formed between C and O. However, there is a five-fold enhancement of the magnetic moment of the surface Ni atoms. With graphone on top, the magnetic moments of the surface Ni(111) atoms with and without the spacer layer are 1 μ_B and 0.19 μ_B, respectively. For the 0.5 ML case we observe that the induced magnetic moment on graphene increases to 0.31 μ_B.

References

[1] K. S. Novoselo *et al. Science* **306**, 666 [2004].

[2] J. C. Charlier *et al. Topics in Applied Physics Volume 111*, pp 673-709 [2008]

[3] A. H. Castro Neto *et al. Rev. Mod. Phys.* **81**, 109 [2009].

[4] V. M. Karpan *Phys. Rev. Lett.* **99**, 176602 [2007].

[5] J. O. Sofo *et al. Phys. Rev. B* **75**, 153401 (2007).

[6] J. Zhou *et al. Nano Lett.* **9**, 3867 (2009)

[7] Niharika Joshi *et al. PHYSICAL REVIEW B* **86**, 121411(R) (2012)

[8] Paolo Giannozzi *Metodi Numerici in Struttura Elettronica Corso di Laurea in Fisica Computazionale* (2009)

[9] Paolo Giannozzi *Metodi Numerici in Struttura Elettronica Corso di Laurea in Fisica Computazionale* (2009)

[10] Phillip Phillips *Advanced solid state physics* (2003).

[11] Robert G Parr *et al. Density functional theory of atoms and molecules* **142** (1989)

[12] Phillip Phillips *Advanced solid state physics* (2003).

[13] M. C. Payne *et al. Reviews of Modern Physics, Vol. 64* No. 4, (1992)

[14] M. C. Payne *et al. Reviews of Modern Physics, Vol. 64* No. 4, (1992)

[15] P. Hohenberg and W. Kohn, *Phys. Rev.* ,**136** B864 (1964)

[16] W. Kohn and L. Sham, *Phys. Rev.* **147**, A1133 (1965)

[17] Ceperly *et al. Phys. Rev. Lett.***45** , 566 1980

[18] Paolo Giannozzi *Metodi Numerici in Struttura Elettronica Corso di Laurea in Fisica Computazionale* (2009)

[19] Robert G Parr *et al. Density functional theory of atoms and molecules* **142** (1989)

[20] M. C. Payne *et al. Reviews of Modern Physics, Vol. 64* No. 4, (1992)

[21] P. Giannozi *et al. J. Phys: Condens. Matter bf*21, 395502 (2009).

[22] D. Vanderbilt *Phys. Rev. B* **41** 7892-7895 (1990).

[23] J. Perdew, K. Burke, M. Ernzerhof *Phys. Rev. Lett.* **77**, 3865-3868 (1996).

[24] H. Monkhorst and J. *Pack Phys. Rev B* **13**, 5188-5192 (1976).

[25] N. Marzari and D. Vanderbilt *Phys. Rev. Lett.* **82**, 3296-3299 (1999).

[26] C Lazo *et al. PHYSICAL REVIEW B* **79**, 245418 (2009)

[27] Niharika Joshi *et al. PHYSICAL REVIEW B* **86**, 121411(R) (2012)